ELSEVIER

Biophysical Chemistry 133 (2008) 54–65

Biophysical Chemistry

http://www.elsevier.com/locate/biophyschem

Study by optical spectroscopy and molecular dynamics of the interaction of acridine–spermine conjugate with DNA

S. Sánchez-Carrasco [a], J.G. Delcros [b], A.A. Moya-García [c], F. Sánchez-Jiménez [c], F.J. Ramírez [a,*]

[a] *Departamento de Química Física, Facultad de Ciencias, Universidad de Málaga, Campus de Teatinos, 29071 Málaga, Spain*
[b] *Groupe de Recherche en Thérapeutiques Anticancéreuses, UPR ESA CNRS 6027, Faculté de Medecine, Université de Rennes I, 2 Avenue du Professeur Léon Bernand, 35043 Rennes Cédex, France*
[c] *Departamento de Biología Molecular y Bioquímica, Facultad de Ciencias, Universidad de Málaga, Campus de Teatinos, 29071 Málaga, Spain*

Received 24 October 2007; received in revised form 12 December 2007; accepted 13 December 2007
Available online 23 December 2007

Abstract

We report a spectroscopic and theoretical study of the interaction between double-stranded oligonucleotides containing either adenine–thymine or guanine–cytosine alternating sequences and N1-(Acridin-9-ylcarbonyl)-1,5,9,14,18-pentazaoctadecane, or ASC, which is formed by the covalent bonding of spermine and 9-amidoacridine moieties via a trimethylene chain. Solutions containing the oligonucleotides and the conjugate at different molar ratios were studied using complementary spectroscopic techniques, including electronic absorption, fluorescence emission, circular dichroism, and Raman spectroscopy. The spectroscopical properties of ASC at both the vibrational and the electronic levels were described by means of *ab initio* quantum-chemical calculations on 9-amidoacridine, used as a model compound. Molecular dynamics calculations, based on the QM/MM methodology, were also performed using previously docked structures of two oligonucleotide–ASC complexes containing the A–T and the G–C sequence. Our data, taken all together, allowed us to demonstrate that conjugation of spermine to acridine modulates and gives additional properties to the interaction of the latter with DNA. As the ASC molecule has a high affinity by the polyamine transport system, these results are promising for their application in the development of new anti-tumour drugs.

Keywords: Acridine; Spermine; DNA; Spectroscopy; Molecular dynamics

1. Introduction

Acridine is a heteroaromatic molecule able to intercalate into DNA [1]. This structural property confers anti-tumour capabilities to acridine and its derivatives [2], since DNA is the main target in anti-cancer drug design [3,4]. Intercalation of a planar system between DNA base pairs can induce structural alterations in such a way that cell proliferation is blocked [5,6]. A usual mechanism to explain this fact is related to the DNA-binding enzymes which have essential roles in reactions directly involved in cell proliferation, such as topoisomerases and telomerases [7,8]. The DNA-intercalator complexes prevent, in most cases, DNA recognition by these enzymes, thus disrupting the whole process.

It is known that one of the main problems of anti-tumour therapies is the secondary effects caused by the action of cytotoxic drugs on healthy cells. Most of the promising drugs preserve cytotoxic activity, although they have tumour cells as their main target. In the case of intercalators, this selectivity can be acquired by attaching an aliphatic side chain [4,9]. These chemical substituents can also provide both cell-specificities and new contributions to DNA binding, as they can establish additional interactions with intra-cellular reactive sites. As a consequence, changes can appear in the thermodynamic parameters of binding and in useful biochemical properties, such as uptake systems or sequence selectivity. This strategy is being currently tested by functionalizing the acridine molecule [2]. Acridine based anti-tumour drugs have been developed and studied [10,11], as amsacrine or asulacrine, which present excellent activity against

* Corresponding author. Fax: +34 95 2132000.
E-mail addresses: delcros@univ-rennes1.fr (J.G. Delcros), kika@uma.es (F. Sánchez-Jiménez), ramirez@uma.es (F.J. Ramírez).

0301-4622/$ - see front matter © 2008 Elsevier B.V. All rights reserved.
doi:10.1016/j.bpc.2007.12.003

some cases of leukaemia [12]. Acridine derivatives recently synthesized have been proven to stabilize G-quadruplex structures in telomeres, inhibiting telomerase action [13].

The biogenic polyamines are organic polycations essential for cell proliferation [14]. Tumour cells uptake biogenic polyamines in greater amounts than do healthy cells [15,16], thus making them suitable candidates for improving the anti-cancer action of intercalators like acridine. Three important features have been recently proven for a series of acridine–polyamine covalent conjugates [17–21]: i) they present higher affinities for DNA than acridine; ii) they preserve the topoisomerase II inhibitory activity of acridine and, iii) they are recognized by the polyamine transport system. Acridine–polyamine conjugates are, therefore, promising chemical systems for the development of more efficient anti-tumour drugs. Nevertheless, this task requires a deeper knowledge of the structure and binding properties of these molecules [3], which enhances the role of physico-chemical tools in developing anti-cancer drugs and in understanding their structure–activity relationships.

In this work, we used electronic (absorption, fluorescence, circular dichroism) and vibrational (Raman) spectroscopies to investigate the interaction with DNA of a conjugate molecule formed by acridine and spermine bound by means of a trimethylene-amide group (hereafter ASC), Fig. 1. The affinity of spermine to the DNA major groove has been evidenced by different experimental and theoretical studies [22–24]. Here, we will discuss the influence of spermine conjugation on the intercalation of acridine into DNA chains. For the DNA models, we have chosen the 16-mer oligonucleotides ds(dG–dC)$_8$ and ds(dA–dT)$_8$. Comparison between results from these two sequences allowed us to investigate the sequence selectivity in the DNA binding of this compound, as observed for other acridine derivatives with applied interest [25]. Ultraviolet–visible (UV–vis) absorption, emission fluorescence, circular dichroism (CD) and Fourier transform (FT) Raman spectra of solutions containing these oligonucleotides and ASC, at different molar ratios, were recorded. Thermal denaturation experiments in the absence and in the presence of the conjugate were performed on genomic DNA and poly(dA–dT).

In order to support the experimental results, density functional theory (DFT) calculations, using *ab initio* methodology at the 6-31G** level and simulating the solute–solvent electrostatic interactions by means of the polarizable continuum model (PCM), were performed on the molecule 9-(*N*-methylamide)-acridine, as a model compound. These calculations provided us a reliable assignment of the electronic and vibrational transitions of the acridine–spermine conjugate in aqueous solution. Molecular dynamics (MD) calculations of the interaction between the conjugate and both oligonucleotide sequences were also performed on the basis of a hybrid quantum mechanics/molecular mechanics (QM/MM) approach. This methodology allows the conjugate to always be described as a quantum system, while the oligonucleotides are treated with a classical MM force field. The optimized conjugate-oligonucleotide structures for both sequences were validated by the experimental data.

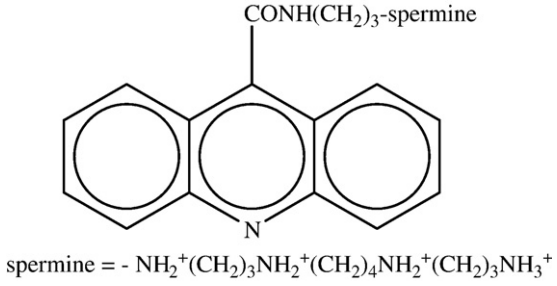

Fig. 1. Chemical structure of the acridine–spermine conjugate (ASC).

2. Experimental

2.1. Materials

Details about the synthesis of N1-(Acridin-9-ylcarbonyl)-1,5,9,14,18-pentazaoctadecane, hereafter referred to as the acridine–spermine conjugate or ASC, are given elsewhere [26]. The single-stranded 16-mer oligonucleotides ss(dG–dC)$_8$ and ss(dA–dT)$_8$, calf-thymus genomic DNA and poly-ds(dA–dT) were synthesized by Sigma Chemical Co. Double-stranded oligonucleotides, ds(dG–dC)$_8$ and ds(dA–dT)$_8$, were obtained and tested as previously reported [27,28]. To keep conditions close to the physiological environment, 10 mM TRIS buffer, 100 mM sodium chloride, was always used as the solvent. Final pH was adjusted to the physiological value (7.5) by using aqueous hydrochloric acid. Stock solutions of 120 mM (in phosphate) oligonucleotides were stored at 4 °C until ready for use in the experiments. Solutions for different experiments were prepared by dilution of these stock solutions up to the suitable concentration.

2.2. Spectral measurements

UV–vis absorption spectra were recorded in an Agilent 8453 UV-visible spectrophotometer supplied with a diode array detector. The oligonucleotide–conjugate interaction was studied by observing the behavior of the conjugate absorption bands in the visible region, where they are free from oligonucleotide absorptions, while increasing the oligonucleotide concentration, either ds(dG–dC)$_8$ or ds(dA–dT)$_8$. The following general procedure was used: an initial spectrum of a 2 μM ASC solution was recorded; then, 5 1-μl aliquots of an oligonucleotide solution of 40 mM (in phosphate) were sequentially added to increase the concentration until reaching a final titration point of 120 μM without an appreciable change in the total volume; a new spectrum was recorded after each addition. The entire protocol was repeated at least twice for each oligonucleotide, in order to confirm the results. All spectra were recorded at least 10 min after oligonucleotide addition, although the complex was always formed within a few seconds. To improve the separation of peaks and shoulders in overlapping absorption bands, a Fourier self-deconvolution procedure was performed using a standard Gaussian line-broadening function (deconvolution factor 276; suppression factor 0.2). These parameters

allowed suitable resolution of the acridine absorptions in the visible region between 300 and 450 nm.

Thermal denaturing studies were performed in a variable temperature cell Specac P/N 2100 equipped with a Copper–Constanton thermocouple for temperature monitoring purposes. Data were always acquired after thermal equilibrium was reached, which was automatically checked by the acquisition software. Thermal analysis for poly-ds(dG–dC) was not achieved because it does not melt within the range of available temperatures. The melting temperature (T_m) was determined over the A_{260} versus the temperature curves, using the first derivative method. Fluorescence spectra were measured in a Photon Technology International (PTI) spectrofluorimeter. Two kind of experiments were performed for each oligonucleotide. Firstly, the influence of conjugate addition on oligonucleotide-bound ethidium fluorescence was studied. Secondly and separately, the behaviour of the fluorescence emission of ASC in the presence of the oligonucleotides at different molar ratios was studied. In this case, successive fluorescence spectra were recorded following the same titration procedure described previously for the absorption spectra. As previously seen in the corresponding excitation fluorescence spectra, maximal quantum yields were achieved using radiation at 471 nm for ethidium and at 360 nm for ASC. Electronic CD spectra were recorded in a JASCO J-810 spectropolarimeter. Standard quartz cells of 1 or 10 mm path length were used for conjugate concentrations higher or lower than 100 μM, respectively, in order to avoid the detector's overload. Buffer corrections were applied immediately after recording the spectra. The spectra were expressed in terms of molar ellipticity of the oligonucleotide, which was calculated from the equation $[\Theta]=\Theta/cl$ [29]. In this equation Θ is the ellipticity, c is the oligonucleotide molar concentration, and l is the cell pathlength in cm.

FT-Raman spectra of the oligonucleotides, ASC and their complexes were recorded at room temperature (20 °C) by means of a Bruker Equinox 55 spectrometer supplied with a Raman module. Spectra were obtained at a resolution better than 2 cm^{-1}, using excitation radiation wavenumber at 1064 nm from a Nd-YAG laser working at 500 mW. Samples were analysed using a sapphire cell suitable for low volumes of liquid samples. The Raman spectra were recorded using the general procedure previously reported elsewhere [27,28]. To discuss the Raman peaks, the following selection criteria were adopted: i) peaks must appear with the same wavenumber and intensity in the spectra of independent samples; ii) peaks must exhibit an intensity clearly higher than the experimental noise level; and iii) peaks should be previously reported and assigned in the literature. Spectral treatment was performed using the Bruker OPUS © spectroscopic software. All the Raman spectra were normalized to the sapphire band at 750 cm^{-1}.

2.3. Theoretical calculations

The GAUSSIAN'03 package of programs [30] was used for DFT quantum-chemical calculations. We used the hybrid functional B3PW91 [31,32], which has been successfully proven to accurately reproduce structural and spectroscopic features of biological molecules [33–35]. To simulate an aqueous environment, a PCM was employed [36,37].This model places the solute molecule into a size-adapted cavity formed from interlocking atom-centered van der Waals spheres, while the solvent is assimilated into a continuum characterized by its dielectric constant (78.7 for water).

Spectroscopic features were computed on the optimized molecular structure, which was obtained by allowing all the geometric parameters to vary independently. Electronic excitation energies were obtained by using time-dependent (TD) formalism [38,39]. Quadratic force constants were calculated from the analytical second derivatives of the molecular energy with respect to the Cartesian coordinates, in the geometry of minimal energy. Raman intensities were calculated by numerical differentiation of dipole derivatives with respect to the electric field. The theoretical Raman spectrum was obtained from the calculated vibrational wavenumbers and the Raman intensities. Every Raman band was represented by a Gaussian function of 20 cm^{-1} half-height width.

We used the split-valence 6-31G** basis set [40,41], which includes six s-type and three p-type polarization functions, for structural optimization, contour surfaces and time-dependent calculations. Force field, vibrational wavenumbers, Raman intensities and normal coordinates were computed using the 3-21G* basis set, with only s-type polarization functions, over the 6-31G** optimized geometry. The use of polarization functions is necessary in order to correctly describe the solute–solvent interactions, because they allow for a suitable charge distribution adapted to the presence of an external electric field, such as a polar environment.

Docking calculations were performed using the GRAMM (Global Range Molecular Matching) v1.03 program [42]. This is a fast Fourier transform based method that works from the atomic coordinates of the two interacting systems, without requiring any additional information about the binding sites. The structure of the complex is achieved after a systematic six-dimensional grid search through the relative molecular rotations and translations. Atomic coordinates of the ASC and the oligonucleotides were obtained in different ways. The ASC geometry of minimal energy was obtained using the GAUSSIAN'03 package at the same level of calculation previously described, although not including solvent effects. Atomic coordinates for the oligonucleotides were obtained from standard structural parameters for nucleic acids using the HyperChem program [43].

The two better-scored intercalated ASC–oligonucleotide structures, one for each sequence, were used as starting points of a deeper theoretical study based on QM/MM hybrid methodology. Once the initial interaction was defined, the complete system was placed in a $68\times47\times42$ Å side box of water molecules, from which molecules overlapping with ASC or the oligonucleotides were removed. The simulation box also contained sodium ions to compensate for the negative charges of the ASC–oligonucleotide complex, resulting in an electrically neutral system hydrated with 1284 water molecules. The full system was described using a hybrid QM/MM Hamiltonian. The ASC molecule was the quantum sub-system, being treated

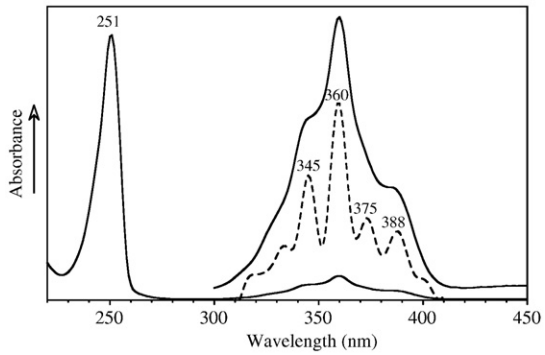

Fig. 2. Electronic absorption spectra of ASC (solid lines) and deconvoluted spectra (dotted line).

using the semiempirical Hamiltonian AM1 [44]; the oligonucleotides, water molecules and sodium ions were the classical sub-system, being treated at a MM level. To describe the oligonucleotide sequences, we used the CHARMM force field as developed by MacKerell et al. [45,46], whereas we used a flexible TIP3P potential for water molecules [47]. Sodium ions and van der Waals parameters of the ASC molecule were also taken from the CHARMM force field [48].

Once the material model was defined, we were ready to study the behaviour of the two ASC–oligonucoleotide models. A detailed theoretical protocol has been included as Supplementary Material. All calculations were made with the CHARM31 program [48]. We employed periodic boundary conditions and a switched cut-off radius of 10 Å for all types of interactions. The bond lengths of all hydrogen atoms of the classical sub-system were kept constrained to their equilibrium lengths using the SHAKE algorithm [49]. MD simulations were carried out using the leap-frog [50] integration algorithm with a time step of 1 fs.

3. Results and discussion

3.1. Results obtained from the spectral measurements

The spectrum of ASC in the absence of oligonucleotides is shown in Fig. 2. It exhibits two band systems: a very strong absorption in the UV region, centred at 251 nm (which has a second component observed as a shoulder at a higher energy), and a more complex system in the visible region with a maximum at 360 nm. Fourier self-deconvolution enabled us to obtain the main components of this broad band, which were measured at 345, 375 and 388 nm. This medium-intensity multiplet presents the advantage of being free of the oligonucleotide absorptions which appear at lower wavelengths. This region, therefore, is suitable for monitoring the conjugate–oligonucleotide interaction. In order to provide a supported assignment of these bands, we carried out a theoretical prediction of the electronic excitation energies. Taking into account that the electronic absorption in the visible region should correspond to $\pi\rightarrow\pi^*$ and $n\rightarrow\pi^*$ transitions [51,52], TD calculations were carried out on the 9-(*N*-methyl-amide)-acridine molecule. The results concerning the calculated energies of the electronic transitions and their assignments in terms of the frontier

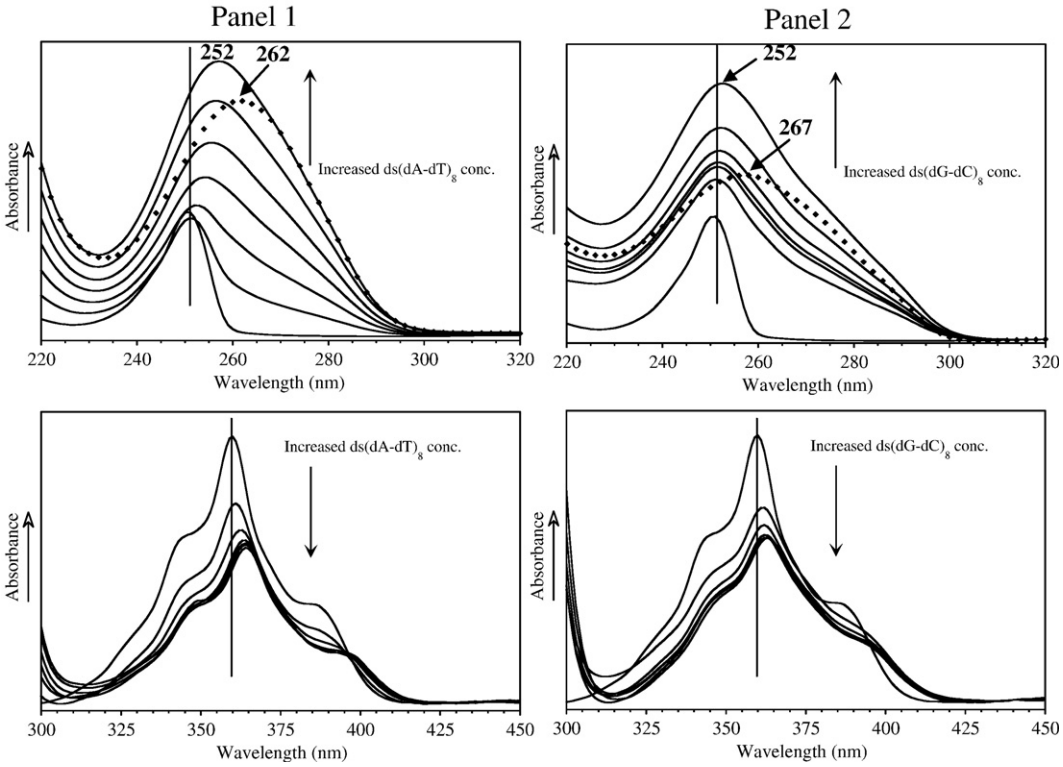

Fig. 3. Electronic absorption spectra in the visible region of solutions 2 μM ASC and increased concentrations of the oligonucleotides up to 120 μM. The oligonucleotide concentration increment in each step was 20 μM. Panel 1: ds(dA–dT)$_8$. Panel 2: ds(dG–dC)$_8$.

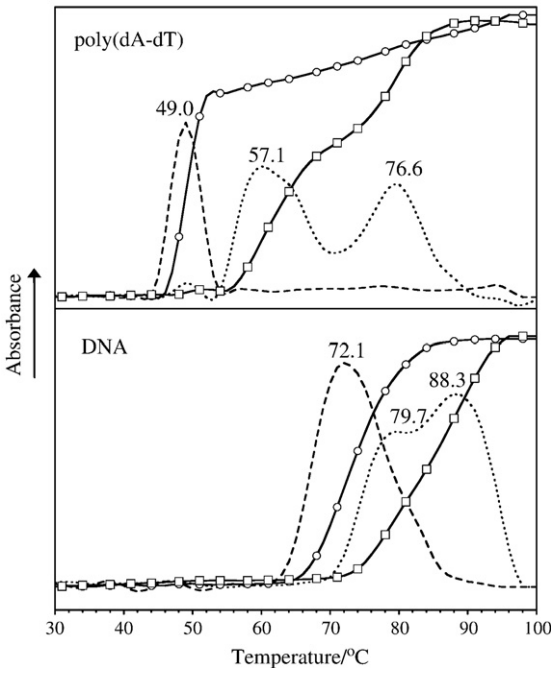

Fig. 4. Thermal denaturing curves from the electronic absorbance at 260 nm (solid lines) of poly-ds(dA–dT)$_8$ and ct DNA, both at a concentration 60 μM in phosphate, alone (circles) and in the presence of 3 μM ASC (squares). Temperature increment was 2 or 0.5 °C for wavelength regions far or around the melting region, respectively. First derivatives of the thermal denaturing curves are represented as dashed (free) and dotted (with 3 μM ASC) curves.

molecular orbitals are available as Supplementary Material. The calculated wavelengths fit well to the experimental values, and the assignments indicate that the band system between 300 and 400 nm observed in the ASC electronic absorption spectrum involves a partial charge-transfer from the amide group to the acridine ring.

We have displayed in Fig. 3 (Panel 1) the effect of the oligonucleotide addition in the electronic spectrum of ASC between 300 and 400 nm. A table containing the relevant wavelength changes has been included as Supplementary Material. Both figures show strong hypochromism and a red-shift of the absorption maxima of ASC when increasing the oligonucleotide concentration. The titration with ds(dA–dT)$_8$ also shows an isosbestic point at 393 nm, which was not observed for ds(dG–dC)$_8$. On the other hand, 73% and 65% of the final hypochromism of the 360 nm band were measured in the first titration step for ds(dA–dT)$_8$ and ds(dG–dC)$_8$, respectively, that is to say, at an ASC:oligonucleotide molar ratio of 3:1. The Fig. 3 (Panel 2) also shows the behaviour of the electronic spectra of the oligonucleotides near 260 nm. In the two cases, the absorption bands increase during the titration. However, the 262 nm band of ds(dA–dT)$_8$ shifted from 252 to 257 nm in the presence of ASC, while the 257 nm band of ds(dG–dC)$_8$ remained unshifted at 252 nm during the course of the titration.

Melting curves and first derivatives for calf-thymus DNA and poly-ds(dA–dT) are shown in Fig. 4. The curves for DNA

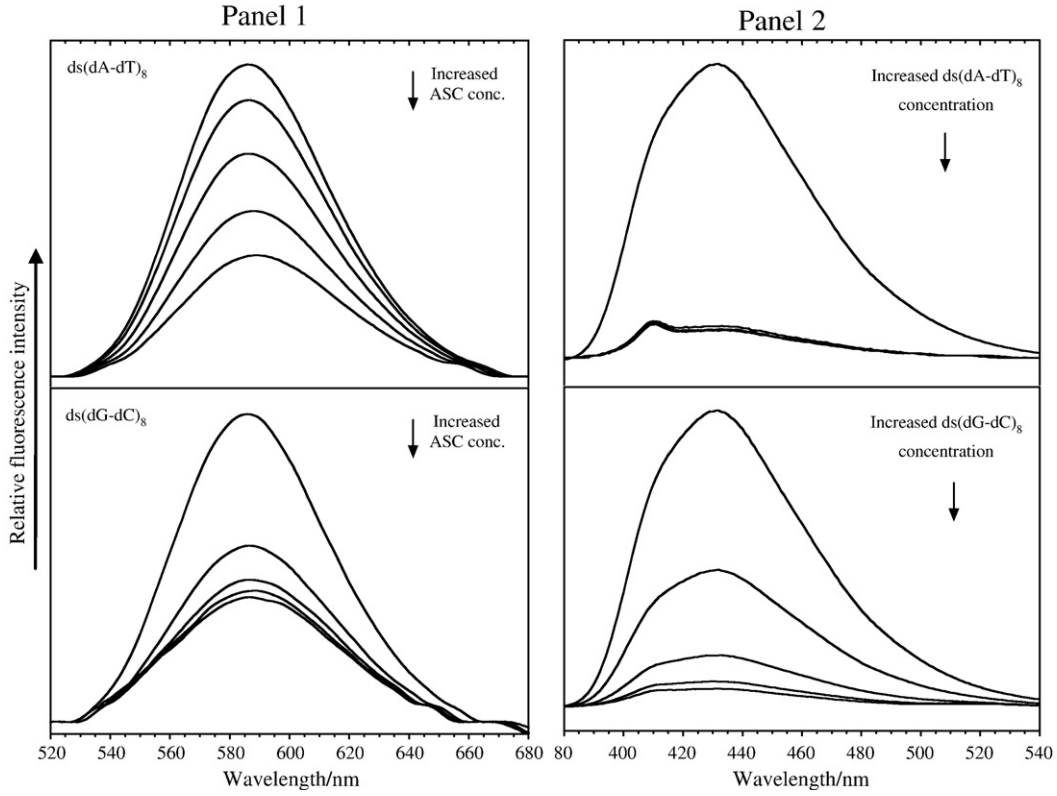

Fig. 5. Panel 1: fluorescence emission spectra of oligonucleotide-intercalated ethidium (2 μM of ethidium and 60 μM, in phosphate, of the oligonucleotides) in the presence of 0, 4 and 8 μM of ASC. Panel 2: fluorescence emission spectra solutions 2 μM ASC in the presence of increased concentrations of the oligonucleotides up to 80 μM. The oligonucleotide concentration increment in each step was 20 μM.

in the presence of ASC exhibit two transitions associated with the melting process, namely, at 79.7 and 88.3 °C, which appear respectively at temperatures 7.6 and 16.2 °C higher than the melting point of the DNA alone (72.1 °C using our experimental settings). In the case of poly-ds(dA–dT), a third transition was observed at 76.6 °C, together with two close melting transitions, one at 57 °C and a second at a higher temperature.

Fig. 5 (Panel 1) shows lowering of the fluorescence emission band of oligonucleotide-bound ethidium with increasing concentrations of ASC for ds(dG–dC)$_8$ and ds(dA–dT)$_8$. However, in the presence of ds(dA–dT)$_8$ the intensity reduction is proportional to the increase in the ASC concentration over the whole range of concentrations studied, while the ethidium fluorescence spectra in the presence of ds(dG–dC)$_8$ exhibited a strong quenching (more than 50%) during the first titration step, while further ASC additions induced smaller changes. The emission spectra of ASC alone and in the presence of increasing amounts of the oligonucleotides are displayed in Fig. 5 (Panel 2), which shows how the addition of oligonucleotides gives rise to a dramatic reduction in the fluorescence intensity of ASC, together with changes to the spectral profiles. The fluorescence quenching was similar over the range of the ASC:ds(dA–dT)$_8$ molar ratios analysed. However, the first addition of ds(dG–dC)$_8$ only induced a 53.4% intensity reduction with respect to the emission of ASC alone, the relative quenching values for the following steps being 83.7%, 91.5% and 94.1%.

CD spectra of ds(dG–dC)$_8$ and ds(dA–dT)$_8$ alone and in the presence of ASC are shown in Fig. 6. The presence of ASC at concentrations lower than 100 μM in the solution of ds(dA–dT)$_8$ induced several changes in the CD spectrum of this sequence. The positive band at 271 nm shifted upwards to 275 nm; the negative band at 250 nm was enhanced in the solutions at 10 and 25 μM of ASC, being measured at 254 and 253 nm, respectively. The positive band at 219 nm changed to a weak negative feature at 215 nm for the solutions at an ASC concentration of 10 μM. The addition of ASC to the solution of ds(dG–dC)$_8$ gave rise to a biphasic CD signal with a positive band at 262 nm and a negative band at 247 nm. The oligonucleotide positive feature at 285 nm remained unchanged, while the negative band at 253 nm apparently disappeared or was hidden behind the new CD signals. When the ASC concentration reached 250 μM, the CD spectra of the two oligonucleotides exhibited a strong intensity increase as the main feature.

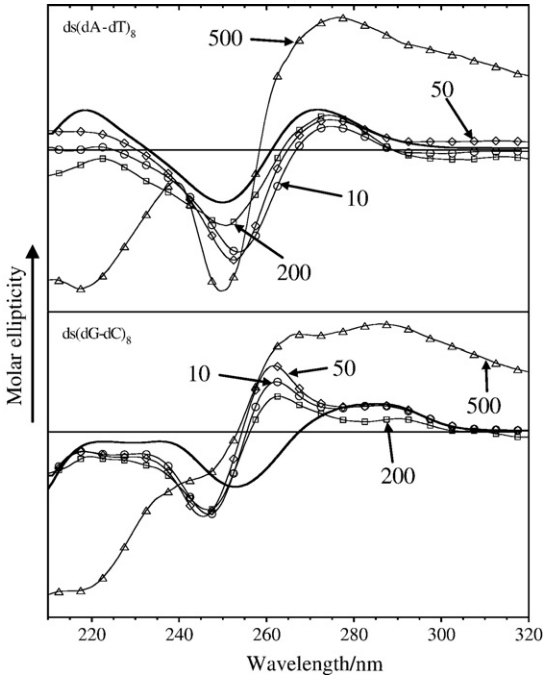

Fig. 6. Electronic CD spectra of the oligonucleotides (60 μM in phosphate) in the presence of different concentrations of ASC: 10 μM (circles), 50 μM (diamonds), 200 μM (squares) and 500 μM (triangles). Solid lines are the spectra in absence of ASC.

The Raman spectra of aqueous solutions containing the oligonucleotides alone and in the presence of either 3 and 10 mM of ASC are shown in Fig. 7. Wavenumbers for the more relevant bands and their assignments are summarized in Tables 1 and 2, which correspond to ds(dA–dT)$_8$ and ds(dG–dC)$_8$, respectively. Under our experimental settings, the solutions of ds(dA–dT)$_8$ were transparent and presented a relatively high fluidity. The assignments of the oligonucleotide Raman bands are based on vibrational studies reported for the polymer, and they have been widely discussed elsewhere [27,28]. The assignments of the ASC bands have been based on a force field and the same normal coordinate calculations for the molecule as the electronic structure calculations, using DFT methodology at the 6-31G** level. A set of the obtained theoretical vibrational data has been included as Supplementary Material.

3.2. Analysis and discussion of the spectral results

The aforementioned spectral data support the following conclusions:

1. The acridine moieties of ASC can intercalate between adjacent base pairs of oligonucleotide sequences. The first evidence of this conclusion is found in the hypochromism and red-shift observed by UV–vis absorption spectroscopy, Fig. 3. ASC is also able to displace ethidium from its intercalation sites in oligonucleotides, as shown in the Fig. 5. The observed splittings of the phosphodioxy stretching band in the Raman spectra of both ds(dA–dT)$_8$ and ds(dG–dC)$_8$ are also a consequence of the structural re-organization of the double-helix upon acridine intercalation.
2. One 16-mer double-stranded chain can host more that one ASC molecule by intercalation. This fact is evidenced by comparing the intensity reduction of the ASC electronic absorption band in the initial steps of the titrations, that is to say, when an excess of conjugate is present. Thus, we measured 73% and 65% of the final hypochromism for ds(dA–dT)$_8$ and ds(dG–dC)$_8$, respectively, in the first oligonucleotide addition, which corresponds to an oligonucleotide:ASC molar ratio of 1:3. A similar behaviour was observed in the fluorescence spectra showed in the Fig. 5, thus supporting this assertion.

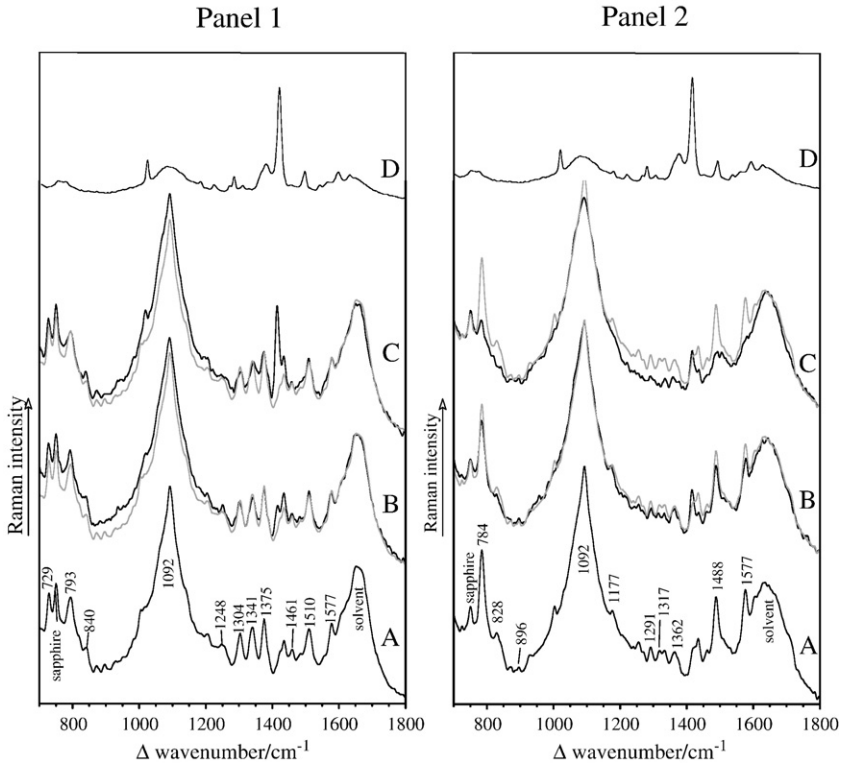

Fig. 7. Raman spectra of solutions (A) 60 mM oligonuleotide, in phosphate; (B) 60 mM oligonuleotide and 3 mM ASC; (C) 60 mM oligonuleotide and 10 mM ASC; (D) 60 mM ASC. Panel 1: ds(dA–dT)$_8$. Panel 2: ds(dG–dC)$_8$. The solutions were prepared by mixing 1.5 μl of oligonucleotide stock solutions (120 mM in phosphate) with 1.5 μl of ASC, at concentrations either 6 or 20 mM.

3. The isosbestic point at 393 nm observed in Fig. 3 indicates the existence of a conformational equilibrium between bonded and free ASC molecules during the titration with ds(dA–dT)$_8$. The thermal denaturing curves, Fig. 4, exhibit structured profiles for both poly-ds(dA–dT) and calf-thymus DNA. These profiles are explained as the result of at least two melting processes [53,54]. The first of them would be a partial opening of the helix near the occupied sites, accompanied by a redistribution of the bound ligands to allow the helix to melt in larger loops. In second process, the ligands are removed from the helix before complete melting. However, it has been

Table 1
Wavenumbers and assignments for relevant bands measured in the Raman spectra of solutions 60 mM ds(dA–dT)$_8$, in phosphate, and different concentrations of ASC

ds (dA–dT)$_8$	ds(dA–dT)$_8$ 3 mM ASC	ds(dA–dT)$_8$ 10 mM ASC	ASC	Assignments[a]
		1594	1596	Acridine, ν(arom)
1577	1577	1580		Adenine (C6-NH_2, N3)
		1538	1541	Acridine, ν(arom)
1510	1510	1509		Adenine
	1495	1495	1495	Acridine, δ(C–H)+ν(arom)
1461	1459	1458		Deoxyribose
	1416	1415	1418	δ(CH_2)
		1384	1379	Amide III+ν(arom)
1375	1375			Thymine (CH_3),
1341	1342	1344		Adenine
		1306	1308	Acridine, δ(C–H)
1304	1301	1301		Adenine, thymine
		1280	1282	ν(arom)+δ(C–H)
1248	1251			Adenine (C6–NH_2), thymine
1092	1092	1092		Phosphodioxy
	1021	1018	1021	Acridine, δ(C–H)
840	840/832	839		Phosphodiester,deoxyribose
793	793	793		Phosphodiester, thymine
729	727	727		Adenine (N3)

[a] Symbols used: ν (stretching), δ (bending).

Table 2
Wavenumbers and assignments for relevant bands measured in the Raman spectra of solutions containing 60 mM ds(dG–dC)$_8$, in phosphate, alone and in the presence of 3 mM ASC

ds(dG–dC)$_8$	ds(dG–dC)$_8$–ASC	ASC	Assignments[a]
1577	1578		Guanine (N3)
1488	1488		Guanine (N7)
	1416	1418	δ(CH_2)
	1375	1379	Amide III+ν(arom)
1362	1364		Deoxyribose
1317	1314		Guanine
	1303	1308	Acridine, δ(C–H)
1291	1294		Cytosine
	1218	1221	Acridine, δ(C–H)
1177	1173		Cytosine, guanine
1092	1092		Phosphodioxy
896	896		Phosphodiester, deoxyribose
828	828/816		Phosphodiester
784	784		Phosphodiester, cytosine

[a] Symbols used: ν (stretching), δ (bending).

theoretically demonstrated that multiphasic melting profiles is not always an evidence cooperative binding [54]. On the other hand, the observed increases of the melting points indicate stabilization of the duplexes, which is a usual characteristic of groove interaction.

4. Evidence of the interaction of the spermine tails with the double-helix grooves was found in the very intense bands measured in the CD spectra of the oligonucleotides at ASC concentrations of 250 μM. These intensity increase are distinctive of cholesteric liquid-crystal structures named Ψ-DNA [55–59]. They are highly ordered structures which give rise to long-range interactions between the base pairs and, as a consequence, strong increases of the oligonucleotide CD bands [60,61].
5. The interactions of ASC with ds(dA–dT)$_8$ and ds(dG–dC)$_8$ exhibited different spectroscopic features, which can indicate base selectivity. The main features which support this point are the following:
   i) The melting curves of poly-ds(dA–dT) and DNA behave differently with the presence of ASC.
   ii) The UV-absorption titrations of ASC exhibit differences with respect of the base sequence (hypochromism, behaviour of the main oligonucleotide absorption band, presence of isosbestic points).
   iii) ASC is able to remove more efficiently ethidium from ds(dG–dC)$_8$ than from ds(dA–dT)$_8$.
   iv) The quenching of the fluorescence of ASC when adding ds(dA–dT)$_8$ is noticeably different to that observed for ds(dG–dC)$_8$.
   v) The CD spectra of ds(dG–dC)$_8$ in the presence of ASC exhibit a biphasic signal which has been assigned to the acridine moieties placed in a chiral environment (the intercalation sites). This phenomenon was not observed for ds(dA–dT)$_8$.

The Raman spectra, Fig. 7, allowed us to extend the structural details known so far on the ASC–oligonucleotide complexes. The measured wavenumber shifts for the ds(dA–dT)$_8$ Raman bands at 1248 and 729 cm^{-1} could be due to the interaction of the spermine side chain with reactive sites of the bases of the oligonucleotide grooves. This hypothesis is also supported by the most intense ASC Raman band, measured at 1418 cm^{-1}, which has been assigned to a methylene bending vibration of the side chain, $\nu(CH_2)$, scissoring. It appeared at 1416 cm^{-1} in the Raman spectrum of the ds(dA–dT)$_8$ solution, 3 mM in ASC. The ds(dA–dT)$_8$ band at 1577 cm^{-1} was measured at 1580 cm^{-1} at 10 mM ASC. This band involved relevant contributions from both the C(6)–NH_2 bending vibration (major groove) and aromatic stretching modes in which the N(3) atom (minor groove) presents a significant vibrational amplitude [62]. Interaction with adenine was also supported by the ds(dA–dT)$_8$ band at 1341 cm^{-1}, which has been assigned to a stretching vibration of the purine moieties [63,64]. It also shifted upwards by adding 10 mM ASC, similar to the 1577 cm^{-1} band. Upshifting of a stretching vibration is evidence of stronger bonds, which are often accompanied by downshifting of the related bending modes [65]. Here, this fact was observed for the purine bending vibration at 729 cm^{-1}, which is considered to be an adenine marker band [63,66] being measured at 727 cm^{-1} in the presence of 10 mM ASC.

Interaction of the spermine tail of ASC with the nucleotide bases of ds(dG–dC)$_8$ was supported by the measured shifts in the oligonucleotide bands at 1317 cm^{-1} (guanine), 1219 cm^{-1} (cytosine) and 1177 cm^{-1} (guanine, cytosine) [27,67]. Similar to the ds(dA–dT)$_8$ solutions, the $\delta(CH_2)$ band at 1418 cm^{-1} shifted to 1416 cm^{-1}, while the acridine vibrations measured at 1308 and 1221 cm^{-1} downshifted by 5 and 4 cm^{-1}, respectively. On the other hand, the amide III band at 1379 cm^{-1} exhibited the opposite behaviour of that observed with ds(dA–dT)$_8$, which indicates that the amide group of the intercalated ASC molecules interacts differently in these two sequences. Fig. 7 (Panel 2) shows that a significant intensity reduction of the Raman intensities of both ds(dG–dC)$_8$ and ASC is observed when increasing the ASC concentration to 10 mM. This fact indicates that these molecules are no longer in solution, but a solid phase has appeared as a consequence of the interaction between these two polyelectrolytes. It has been demonstrated that DNA collapse is observed in concentrated DNA solutions (millimolar) regardless of the DNA length [68–70]. Raspaud et al. [68] found an empirical relationship to calculate the minimal counterion concentration required to induce DNA collapse, $C_{ion} = [C_{DNA}]^{0,77 \pm 0.03}$, which was in good agreement with the theoretical predictions. At 60 mM oligonucleotide (in phosphate) this equation predicts a minimal cation concentration between 26.5 and 20.7 mM. Taking into account that ASC is a polycation with a molecular charge near +4 at our experimental settings, this threshold was clearly surpassed at 10 mM ASC concentration (equivalent to almost 40 mM in positive charges), while at 3 mM, the cation concentration (near 12 mM) is still insufficient. The same authors predicted that, upon cation-induced precipitation of DNA or oligonucleotides, polycations are all present in the solid phase, while monovalent cations remain partially in solution. This prediction agrees with the absence of a significant ASC Raman signal at 10 mM ASC upon oligonucleotide precipitation. However, this phenomenon was not observed for the ds(dA–dT)$_8$ sequence, supporting that cation-induced precipitation of DNA and other nucleotide chains cannot be exclusively explained on the basis of charge neutralization, but a significant degree of structural specificity is involved [68,71–74].

3.3. Molecular dynamics calculations

As aforementioned, we performed MD calculations on the basis of a hybrid QM/MM approach in order to find interactional theoretical models in agreement with previous experimental results. Since there is a large conformational flexibility of oligonucleotides, MD simulations are often dependent on the starting structure [75]. In order to build suitable ASC–oligonucleotide starting models, the Protein Data Bank (PDB) [76] provided us with geometric parameters of a drug-intercalated 12-mer double-stranded oligonucleotide. Then, we removed the drug and we substituted the nucleic bases one-to-one to build the two alternating purine–pyrimidine double-stranded sequences, ds

$(dA–dT)_6$ and $ds(dG–dC)_6$, which maintaining the original inter-base hole able to host a planar molecule. The ASC structure was optimized using DFT/6-31G** gas-phase methodology.

High-resolution rigid-body docking calculations were performed for the two ASC–oligonucleotide systems. Up to 1000 matches, using a grid step of 1.7 Å, was scored for each sequence. After removing the matches based on end-chain interactions, the best scored structures for both sequences presented the acridine ring intercalated into the double-helix, as can be seen in Fig. 8. On the other hand, the calculated interactional energy for the best scored complex with $ds(dG–dC)_6$ was higher (in absolute value) than for the one with $ds(dA–dT)_6$. This result is compatible to a deeper interaction of ASC with the G–C sequence, which agrees with the Raman data. However, the lack of torsional flexibility enables interaction of the tail with the reactive sites of the grooves.

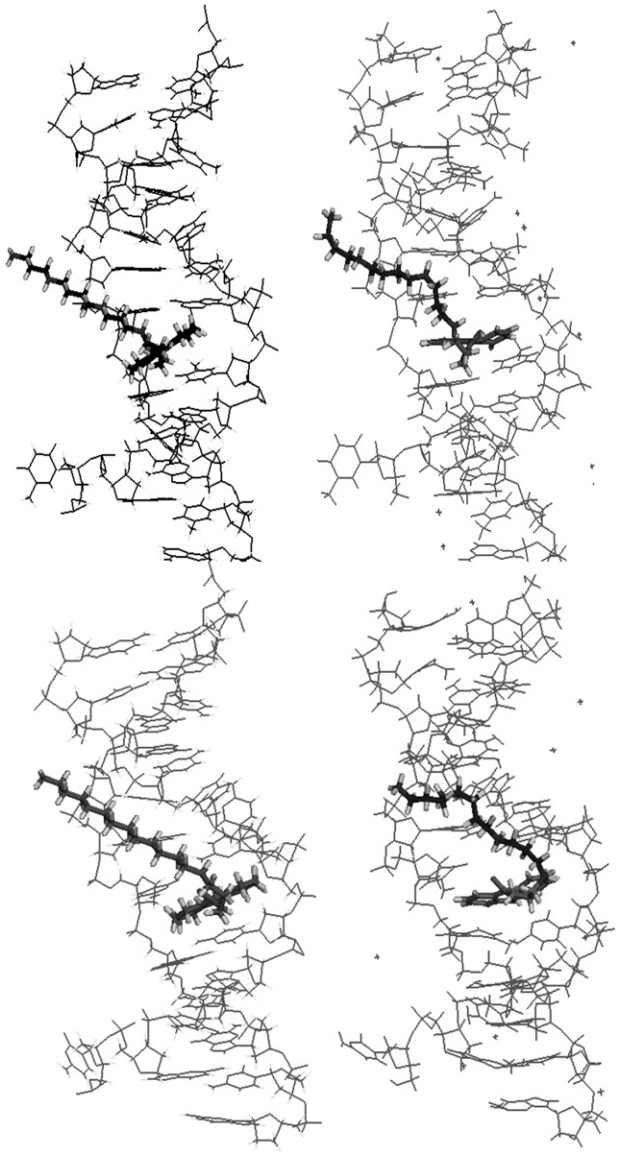

Fig. 8. Comparison between the docked (left) and MD relaxed (right) structures of ASC intercalated into oligonucleotide sequences. Above: $ds(dA–dT)_6$. Below: $ds(dG–dC)_6$.

The stability of the two best scored ASC–oligonucleotide complexes obtained by docking calculations was checked using QM/MM methodology. In both cases, the MD simulations were successful, thus achieving relaxed final structures. They are shown in Fig. 8. As it can be observed, the two final complexes exhibit a fully intercalated acridine ring. Three main common facts can be pointed out: i) conformational changes of the bases in the hole, ii) appreciable out-of-plane deviations of the acridine moieties, and iii) adaptation of the spermine tail to the oligonucleotide groove to achieve additional interatomic contacts. The highest deviations measured for the dihedral angles within the acridine ring were 24 and 21° for the complexes with $ds(dA–dT)_6$ and $ds(dG–dC)_6$, respectively.

The optimized complexes ASC–$ds(dA–dT)_6$ shows the acridine ring deeply intercalated into the double-helix. As a consequence, it is able to interact with the two adenine–thymine base pairs of the hole. The Watson–Crick hydrogen bonding is broken in the hole, which allows the amide group of ASC to interact with the adenine-N1 atom. The H···N1 calculated distance is 1.98 Å, which is within the range of a medium-intensity hydrogen bond [77]. In addition, the oxygen atom of the amide group has captured one acidic hydrogen atom of the second NH_2^+ group of spermine. These interactions agree with the observed Raman shift of 5 cm^{-1} for the amide III band of ASC at 1379 cm^{-1}. The C(6)–NH_2 moieties of the two adenine bases of the hole have rotated their amino groups by about 90° with respect to their starting positions, which is well correlated with the observed behaviour for the oligonucleotide Raman band at 1577 cm^{-1}. As can be easily observed in the Fig. 8, the spermine side chain is adapted to the groove shape, which allows it to establish weak atomic contacts with the phosphate groups and the adenine bases.

The structural specificities of the complex with $ds(dG–dC)_6$ are different than those observed for $ds(dA–dT)_6$. Thus, the π-stacking interaction of the acridine moiety is only clearly established with a purine ring within the hole. This theoretical prediction could explain the observed trends in the fluorescence spectra (Fig. 5). If we accept that the intensity reduction upon intercalation was assigned to a charge-transfer phenomenon between the bases and the ligand, the greater π−stacking predicted for acridine with the bases of the adenine–thymine oligonucleotide will give rise to a more efficient charge-transfer. As a consequence, quenching of the ASC fluorescence will be more intense, as observed in the Fig. 5. On the other hand, the amide group of ASC interacts through the hydrogen atom with a cytosine-N3 atom (1.90 Å), which has also lost its hydrogen bond with the corresponding guanine base. In this case, no hydrogen migration was predicted, which can be well correlated with the different response shown by the amide band at 1379 cm^{-1} of ASC, depending on the oligonucleotide sequence. The side chain deviation from the linear structure was greater in the complex with $ds(dG–dC)_8$. As a consequence, stronger hydrogen bonds are established, which involve a guanine-O6 atom (1.66 Å) and a phosphate moiety (1.64 Å). This result is relevant because a strong interaction of the polycationic tail is required to induce oligonucleotide condensation at high ASC concentrations, as demonstrated by Raman spectroscopy.

4. Conclusions

In summary, our results present a coherent set of experimental and theoretical data aimed at finding new insights about the interaction of DNA with intercalator drugs. In this study we have obtained new insights on preferential binding sites of the acridine–spermine conjugate. Our results indicate that the spermine tail modulates the interaction of acridine with oligonucleotide chains. This interaction appears as base sequence dependent, which was not previously reported for acridine. Our findings support the possibilities of these new molecules to be applied to anti-tumor pharmacology and biotechnology, since they add several specific characteristics provided by the polyamine moiety to the previously described interesting properties of acridine derivatives. Thus, we can postulate a potential application as stabilizers of GC-containing sequences, maybe blocking their ability to be substrates (or ligands) of essential DNA-modifying enzymes (proteins). Further efforts, coming from biophysics and molecular biology, will be necessary to complete the characterization of the potential usefulness of these compounds.

Acknowledgements

The Spanish Ministry of Science and Technology, grants CTQ2006-00686/BQU and SAF2005-01812, has supported this work. The authors greatly thank Prof. I.S. Blagbrough for supplying the acridine–spermine conjugate. We would also like to thank COST-922 (ESF) program and PAI (research groups FQM-159 and CVI-267) for the financial support.

References

[1] A. Albert, The Acridines, Edward Arnold Ltd., London, 1996.
[2] M. Demeunynck, F. Charmantray, A. Martelli, Interest of acridine derivatives in the anticancer chemotherapy, Curr. Pharm. Des. 7 (2001) 1703–1724.
[3] S. Neidle, D.E. Thurston, Chemical approaches to the discovery and development of cancer therapies, Nat. Rev., Cancer 5 (2005) 285–296.
[4] D.E. Graves, L.M. Velea, Intercalative binding of small molecules to nucleic acids, Curr. Org. Chem. 4 (2000) 915–929.
[5] L.A. McDonald, G.S. Eldredge, L.R. Barrows, C.M. Ireland, Inhibition of topoisomerase II catalytic activity by pyridoacridine alkaloids from a *Cystodytes* sp. ascidian: a mechanism for the apparent intercalator-induced inhibition of topoisomerase II, J. Med. Chem. 37 (1994) 3819–3827.
[6] N. Dias, U. Jacquemard, B. Baldeyrou, C. Tardy, A. Lansiaux, P. Colson, F. Tanious, W.D. Wilson, S. Routier, J.Y. Mérour, C. Bailly, Targeting DNA with novel diphenylcarbazoles, Biochemistry 43 (2004) 15169–15178.
[7] A.K. Larsen, A.E. Escargueil, A. Skladanowski, Catalytic topoisomerase II inhibitors in cancer therapy, Pharmacol. Ther. 99 (2003) 167–181.
[8] E. Marco, W. Laine, C. Tardy, A. Lansiaux, M. Iwao, F. Ishibashi, C. Bailly, F.J. Gago, Molecular determinants of topoisomerase I poisoning by Lamellarins: comparison with camptothecin and structure–activity relationships, Med. Chem. 48 (2005) 3796–3807.
[9] H. Andrew, J. Wang, Structure–activity studies of anthracycline-DNA complexes, in: S. Neidle, M. Waring (Eds.), Molecular aspects of anticancer drug–DNA interactions, CRC Press, Boca Raton, Florida, 1993, Chap. 2.
[10] A.S. Delisha, X. Xu, S.D. Thomas, D.M. Miller, Acridine-modified, clamp-forming antisense oligonucleotides synergize with cisplatin to inhibit c-Myc expression and B16-F0 tumor progression, Nucleic Acids Res. 30 (2002) 2565–2574.
[11] B.C. Baguley, L.P. Wakelin, J.D. Jacintho, P. Kovacic, Mechanisms of action of DNA intercalating acridine-based drugs: how important are contributions from electron transfer and oxidative stress? Curr. Med. Chem. 10 (2003) 2643–2649.
[12] N.T. Sklarin, P.H. Wiernik, W.R. Grove, L. Benson, A. Mittelman, J.A. Maroun, J.A. Stewart, F. Robert, J.H. Doroshow, P.J. Rosen, J. Jolivet, J.C. Ruckdeschel, N.J. Robert, E. Velez-Garcia, D.E. Bergsagel, L.C. Panasci, A.M. Van der Merwe, J.J. Longueville, J. Leiby, A phase II trial of CI-921 in advanced malignancies, Invest New Drugs. 10 (1992) 309–312.
[13] R.J. Harrison, J. Cuesta, G. Chessari, M.A. Read, S.K. Basra, A.P. Reszka, J. Morrell, S.J. Gowan, C.M. Incles, F.A. Tanious, W.D. Wilson, L.R. Kelland, S. Neidle, Trisubstituted acridine derivatives as potent and selective telomerase inhibitors, J. Med. Chem. 46 (2003) 4463–4476.
[14] S.S. Cohen, Molecular effects on internal cellular polymers: transfer RNA and DNA, A guide to the polyamines, Oxford Univ. Press, New York, 1998.
[15] T. Thomas, T.J. Thomas, Polyamines in cell growth and cell death: molecular mechanisms and therapeutic application, Cell. Mol. Life Sci. 58 (2001) 244–258.
[16] U. Bachrach, Polyamines and cancer: minireview article, Amino Acids 26 (2004) 307–309.
[17] I.S. Blagbrough, S. Taylor, M.L. Carpenter, V. Novoselskiy, T. Shamma, I.S. Haworth, Asymmetric intercalation of N1-(acridin-9-ylcarbonyl) spermine at homopurine sites of duplex DNA, Chem. Commun. 1998 (1998) 929–930.
[18] O. Phanstiel IV, H.L. Price, L. Wang, J. Juusola, M. Kline, S.M. Shah, The effect of polyamine homologation on the transport and cytotoxicity properties of polyamine-(DNA-Intercalator)conjugates, J. Org. Chem. 65 (2000) 5590–5599.
[19] L. Wang, H.L. Price, J. Juusola, M. Kline, O. Phanstiel IV, The influence of polyamine architecture on the transport and topoisomerase II inhibitory properties of polyamine DNA-intercalator conjugates, J. Med. Chem. 44 (2001) 3682–3691.
[20] S. Carrington, J. Renault, S. Tomasi, J-C. Corbel, P. Uriac, I.S. Blagbrough, A novel solid-phase reductive alkylation route to acridine and dansyl polyamine conjugates, Chem. Commun. (1999) 1341–1342.
[21] N. Seiler, J.G. Delcros, J.Ph. Moulinoux, Polyamine transport in mammalian cells. An update, Int. J. Biochem. Cell Biol. 28 (1996) 843–861.
[22] J. Ruiz-Chica, M.A. Medina, F. Sánchez-Jiménez, F.J. Ramírez, Fourier transform Raman study of the structural specificities on the interaction between DNA and biogenic polyamines, Biophys. J. 80 (2001) 443–454.
[23] B.G. Feuerstein, N. Pattabiraman, L.J. Marton, Molecular mechanics of the interactions of spermine with DNA: DNA bending as a result of ligand binding, Nucleic Acids Res. 18 (1990) 1271–1282.
[24] H.R. Drew, R.E. Dickerson, Structure of a B-DNA dodecamer. III. Geometry of hydration, J. Mol. Biol. 151 (1981) 535–556.
[25] A. Adams, Crystal structures of acridine complexes with nucleic acids, Med. Chem. Rev. 1 (2004) 405–412.
[26] J.G. Delcros, S. Tomasi, S. Carrington, B. Martin, J. Renault, I.S. Blagbrough, P. Uriac, Effect of spermine conjugation on the cytotoxicity and cellular transport of acridine, J. Med. Chem. 45 (2002) 5098–5111.
[27] J. Ruiz-Chica, M.A. Medina, F. Sánchez-Jiménez, F.J. Ramírez, Raman study of the interaction between polyamines and a GC oligonucleotide, Biochem. Biophys. Res. Commun. 285 (2001) 437–446.
[28] J. Ruiz-Chica, M.A. Medina, F. Sánchez-Jiménez, F.J. Ramírez, Raman spectroscopy study of the interaction between biogenic polyamines and an alternating AT oligodeoxyribonucleotide, Biochim. Biophys. Acta 1628 (2003) 11–21.
[29] G. Snatzke, Circular dichroism: an introduction, in: N. Berova, K. Nakanishi, R.W. Woody (Eds.), Circular Dichroism. Principles and Applications, Second Edition, Wiley- VCH, 2000.
[30] M.J. Frisch, G.W. Trucks, H.B. Schlegel, G.E. Scuseria, M.A. Robb, J.R. Cheeseman, J.A. Montgomery Jr., T. Vreven, K.N. Kudin, J.C. Burant, J.M. Millam, S.S. Iyengar, J. Tomasi, V. Barone, B. Mennucci, M. Cossi, G. Scalmani, N. Rega, G.A. Petersson, H. Nakatsuji, M. Hada, M. Ehara, K. Toyota, R. Fukuda, J. Hasegawa, M. Ishida, T. Nakajima, Y. Honda, O. Kitao, H. Nakai, M. Klene, X. Li, J.E. Knox, H.P. Hratchian, J.B. Cross, C.

Adamo, J. Jaramillo, R. Gomperts, R.E. Stratmann, O. Yazyev, A.J. Austin, R. Cammi, C. Pomelli, J.W. Ochterski, P.Y. Ayala, K. Morokuma, G.A. Voth, P. Salvador, J.J. Dannenberg, V.G. Zakrzewski, S. Dapprich, A.D. Daniels, M.C. Strain, O. Farkas, D.K. Malick, A.D. Rabuck, K. Raghavachari, J.B. Foresman, J.V. Ortiz, Q. Cui, A.G. Baboul, S. Clifford, J. Cioslowski, B.B. Stefanov, G. Liu, A. Liashenko, P. Piskorz, I. Komaromi, R.L. Martin, D.J. Fox, T. Keith, M.A. Al-Laham, C.Y. Peng, A. Nanayakkara, M. Challacombe, P.M.W. Gill, B. Johnson, W. Chen, M.W. Wong, C. Gonzalez, J.A. Pople, Gaussian 03, Revision B.0, Gaussian, Inc., Pittsburgh PA, 2003.

[31] A.D. Becke, Density-functional exchange-energy approximation with correct asymptotic behaviour, Phys. Rev. 38 (1998) 3098–3100.

[32] J.P. Perdew, Y. Wang, Accurate and simple analytic representation of the electron-gas correlation energy, Phys. Rev., B 45 (1992) 13244–13249.

[33] F.R. Tortonda, J.L. Pascual-Ahuir, E. Silla, I. Tuñon, F.J. Ramírez, Aminoacid Zwitterions in solution: geometric, energetic, and vibrational analysis using density functional theory-continuum model calculations, J. Chem. Phys. 109 (1998) 592–602.

[34] F.J. Ramírez, I. Tuñon, J.A. Collado, E. Silla, Structural and vibrational study of the taumerism of histamine free-base in solution, J. Am. Chem. Soc. 125 (2003) 2328–2340.

[35] J. Ruiz-Chica, M.A. Medina, F. Sánchez-Jiménez, F.J. Ramírez, On the interpretation of Raman spectra of 1-aminooxy-spermine/DNA complexes, Nucleic Acids Res. 32 (2004) 579–589.

[36] S. Miertus, E. Scrocco, J.J. Tomasi, Electrostatic interaction of a solute with a continuum. A direct utilization of ab initio molecular potentials for the prevision of solvent effects, Chem. Phys. 55 (1981) 117–129.

[37] S. Miertus, J. Tomasi, Approximate evaluations of the electrostatic free energy and internal energy changes in solution, Chem. Phys. 65 (1982) 239–245.

[38] E.K.U. Gross, W. Kohn, Time-dependent density-functional theory, Adv. Quantum Chem. 21 (1990) 255–291.

[39] M.E. Casida, Time-dependent density functional response theory for molecules, in: D.P. Chong (Ed.), Recent Advances in Density Functional Methods, Part I, World Scientific, Singapore, 1995.

[40] T. Clark, J. Chandrasekhar, G.W. Spitznagel, P.J. Schleyer, Efficient diffuse function-augmented basis sets for anion calculations III. The 3-21 +G basis set for the elements Li–F, Comput. Chem. 4 (1983) 294–301.

[41] P.C. Hariharan, J.A. Pople, The influence of polarization functions on molecular orbital hydrogenation energies, Theor. Chim. Acta 28 (1973) 213–222.

[42] I.A. Vakser, Protein docking for low-resolution structures, Protein Eng. 8 (1995) 371–377.

[43] HyperChem. Release 5.0, Hypercube, Inc, Ontario, Canada, 1996.

[44] M.J.S. Dewar, E.G. Zoebisch, E.F. Healy, J.J.P. Stewart, Development and use of quantum mechanical molecular models. 76. AM1: a new general purpose quantum mechanical molecular model, J. Am. Chem. Soc. 107 (1985) 3902–3909.

[45] N. Foloppe, A.J. MacKerell Jr., All-atom empirical force field for nucleic acids: 1. parameter optimization based on small molecule and condensed phase macromolecular target data, J. Comput. Chem. 21 (2000) 86–104.

[46] A. MacKerell Jr., N. Banavali, All-atom empirical force field for nucleic acids: 2) Application to molecular dynamics simulations of DNA and RNA in solution, J. Comput. Chem. 21 (2000) 105–120.

[47] W.J. Jorgensen, Chandrasekhar, J. Madura, R. Impey, M. Klein, Comparison of simple potential functions for simulating liquid water, J. Chem. Phys. 79 (1983) 926–935.

[48] B. Brooks, B. Bruccoleri, B. Olafson, D. States, S. Swaminathan, M. Karplus, CHARMM: a program for macromolecular energy, minimization and dynamics calculations, J. Comput. Chem. 4 (1983) 187–217.

[49] J. Ryckaert, G. Ciccotti, H. Berendsen, Numerical integration of the Cartesian equation of motion of a system with constraints: molecular dynamics of N-alkanes, J. Comput. Phys. 23 (1977) 327–341.

[50] W.C. Swope, H. Andersen, P. Berens, K. Wilson, A computer simulation method for the calculation of equilibrium constants for the formation of physical clusters of molecules: application to small water clusters, J. Chem. Phys. 76 (1982) 637–649.

[51] D. Fornasiero, T. Kurucsev, Analysis of the visible-near-ultraviolet spectrum of 9-aminoacrdine using dichroic spectra in stretched polymer films, Chem. Phys. Lett. 117 (1985) 176–180.

[52] K.E. Van Holde, W.C. Jhonson, P.S. Ho, Principles of Physical Biochemistry, Pretince-Hall, Englewood Cliffs, New Jersey, 1998.

[53] D.M. Crothers, Statistical thermodynamics of nucleic acid melting transitions with coupled binding equilibria, Biopolymers 10 (1971) 2147–2160.

[54] J.D. McGhee, Theoretical calculations of the helix-coil transition of DNA in the presence of large, cooperatively binding ligands, Biopolymers 15 (1976) 1345–1375.

[55] D. Fornasiero, T. Kurucsev, Circular dichroism spectra and the interaction between acridine dyes and deoxyribonucleic acid, Chem. Phys. Lett. 117 (1985) 176–180.

[56] W. Zacharias, J.C. Martin, R.D. Wells, Condensed form of (dG–dC)n′ (dG–dC), as an intermediate between the B- and Z-Type conformations induced by sodium acetate, Biochemistry 22 (1983) 2398–2405.

[57] C.L. Phillips, W.E. Mickols, M.F. Maestreand, L. Tinoco Jr., Circular differential scattering and circular differential absorption of DNA-protein condensates and of dyes bound to DNA-protein condensates, Biochemistry 25 (1986) 7803–7811.

[58] F. Livolant, A.M. Levelut, J. Doucet, J.P. Benoit, The highly concentrated liquid-crystalline phase of DNA is columnar hexagonal, Nature 339 (1989) 457–460.

[59] A. Leforestier, F. Livolant, Liquid crystalline ordering of nucleosome core particles under macromolecular crowding conditions: evidence for a discotic columnar hexagonal phase, Biophys. J. 73 (1997) 1771–1776.

[60] D.M. Gray, I. Tinoco Jr., A new approach to the study of secuence-dependent properties of polynucleotides, Biopolymers 9 (1970) 223–244.

[61] F.J. Ramírez, T.J. Thomas, T. Antony, J. Ruiz-Chica, T. Thomas, Effects of aminooxy analogues of biogenic polyamines on aggregation and stability of calf thymus DNA, Biopolymers 65 (2002) 148–157.

[62] Z. Dhaouadi, M. Ghomi, J.C. Austin, R.B. Girling, R.E. Hester, P. Mojzes, L. Chinsky, P.Y. Turpin, C. Coulombeau, H. Jobic, J. Tomkinson, Vibrational motions of bases of nucleic acids as revealed by neutron inelastic scattering and resonance Raman Spectroscopy. 1. Adenine and its deuterated species, J. Phys. Chem. 97 (1993) 1074–1084.

[63] L. Movileanu, L.M. Benevides, G.J. Thomas Jr., Temperature dependence of the Raman spectrum of DNA. Part I- Raman signatures of premelting and melting transitions of poly(dA–dT)–poly(dA–dT), J. Raman Spectrosc. 30 (1999) 637–649.

[64] L. Movileanu, L.M. Benevides, G.J. Thomas Jr., Temperature dependence of the Raman spectrum of DNA. II Raman signatures of premelting and melting transitions of poly(dA)–poly(dT) and comparison with poly (dA–dT)·poly(dA–dT), Biopolymers 63 (2002) 181–194.

[65] D.W. Mayo, F.A. Miller, R.W. Hannah, Course Notes on the Interpretation of Infrared and Raman Spectra, John Wiley and Sons, Hoboken, NJ, 2004.

[66] M. Katahira, Y. Nishimura, Y. Tsuboi, Y. Sato, Y. Mitsui, Y. Iitaka, Local and overall conformations of DNA double helices with the A–T base pairs, Biochim. Biophys. Acta 867 (1986) 256–267.

[67] J.M. Benevides, G.J. Thomas Jr., Characterization of DNA structures by Raman spectroscopy: high-salt and low-salt forms of double helical poly (dG–dC) in H_2O and D_2O solutions and application to B, Z and A-DNA, Nucleic Acids Res. 11 (1983) 5747–5761.

[68] E. Raspaud, M. Olvera de la Cruz, J.L. Sikorav, F. Livolant, Precipitation of DNA by polyamines: a polyelectrolyte behavior, Biophys. J. 74 (1998) 381–393.

[69] P.G. Arscott, A.Z. Li, V.A. Bloomfield, Condensation of DNA by trivalent cations.1. Effects of DNA length and topology on the size and shape of condensed particles, Biopolymers 29 (1990) 619–630.

[70] D. Porschke, Dynamics of DNA condensation, Biochemistry 23 (1984) 4821–4828.

[71] T.J. Thomas, V.A. Bloomfield, Ionic and structural effects on the thermal helix-coil transition of DNA complexed with natural and synthetic polyamines, Biopolymers 23 (1984) 1295–1306.

[72] M. Saminathan, T. Antony, A. Shirahata, L.H. Sigal, T. Thomas, T.J. Thomas, Ionic and structural specificity effects of natural and synthetic polyamines on the aggregation and resolubilization of single-, double-, and triple-stranded DNA, Biochemistry 38 (1991) 3821–3830.

[73] M. Saminathan, T. Thomas, A. Shirahata, C.K. Pillai, T.J. Thomas, Polyamine structural effects on the induction and stabilization of liquid crystalline DNA: potential applications to DNA packaging, gene therapy and polyamine therapeutics, Nucleic Acids Res. 30 (2002) 3722–3731.

[74] A.J. Geall, D. Al-Hadithi, I.D. Blagbrough, Efficient calf thymus DNA condensation upon binding with novel bile acid polyamine amides, Bioconjug. Chem. 13 (2002) 481–490.

[75] O.M. Becker, M. Watanabe, Dynamics methods, in: O.M. Becker, A.D. Mackerell Jr., B. Roux, M. Watanabe (Eds.), Computational Biochemistry and Biophysics, Marcel Dekker, Inc., New York, 2001.

[76] H.M. Berman, J. Westbrook, Z. Feng, G. Gilliland, T.N. Bhat, H. Weissig, I.N. Shindyalov, P.E. Bourne, The protein data bank, Nucl. Acids Res. 28 (2000) 235–242.

[77] R. Taylor, O. Kennard, Comparison of X-ray and neutron diffraction results for the N–H···O − C hydrogen bond, Acta Crystallogr. B39 (1983) 133–138.